Heliyon 10 (2024) e23498

Contents lists available at ScienceDirect

Heliyon

journal homepage: www.cell.com/heliyon

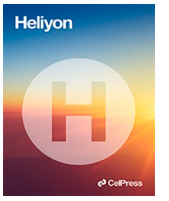

Expression of PD-1 mitigates phagocytic activities TAM in osteosarcoma

Chenhong Zheng [a,1], Heng Li [d,1], Xiaohui Zhao [e,1], Siyu Yang [a], Jinqin Zhan [f], Huaie Liu [g], Yan Jiang [i], Li shi [i], Yaxian Song [i], Yujie Lei [d], Tingdong Yu [d], Xiaoxiong Wang [h], Hongsheng Li [h], Xi Wang [d,***], Yushan Xu [i,**], Zhihong Yao [b,c,*]

[a] *Department of Ultrasound, The Third Affiliated Hospital of Kunming Medical University, Yunnan Cancer Hospital, Kunming, 650118, Yunnan, China*

[b] *Bone and Soft Tissue Tumors Research Centre of Yunnan Province, Department of Orthopaedics, The Third Affiliated Hospital of Kunming Medical University (Yunnan Cancer Hospital), Kunming, Yunnan, 650118, China*

[c] *Department of Cancer Center Office, The Third Affiliated Hospital of Kunming Medical University (Yunnan Cancer Hospital, Yunnan Cancer Center), Kunming, Yunnan, 650118, China*

[d] *Department of Thoracic Surgery I&II, The Third Affiliated Hospital of Kunming Medical University (Yunnan Cancer Hospital), Kunming, Yunnan, 650118, China*

[e] *Department of Ultrasound, Hohhot First Hospital, Hohhot City, 010059, Inner Mongolia Autonomous Region, China Ultrasonic Department, First Affiliated Hospital of Kunming Medical University, Kunming, China*

[f] *Ultrasonic Department, The First Affiliated Hospital of Kunming Medical University, Kunming, Yunnan, 650118, China*

[g] *Department of Geriatric Gastroenterology, The First Affiliated Hospital of Kunming Medical University, Kunming, Yunnan, 650032, China*

[h] *Molecular Diagnostic Center, The Third Affiliated Hospital of Kunming Medical University, Kunming, Yunnan, 650118, China*

[i] *Department of Endocrinology, The First Affiliated Hospital of Kunming Medical University, Kunming, Yunnan, 650118, China*

ARTICLE INFO

Keywords:
Osteosarcoma
PD-1
Tumor-associated macrophages
Metastasis
scRNA-seq

ABSTRACT

The high expression of programmed death 1 (PD-1) is a hallmark of T cell exhaustion, consequently inhibiting the anti-tumor immunity, tumor-associated macrophages (TAMs) aggravate Osteosarcoma (OS) progression. However, PD-1 expression on TAMs in OS metastasis remains unclear. Here, we used scRNA-Seq of 15500 individual cells from human OS lung metastatic lesion, identified thirteen major cell clusters. Our data revealed that tumor-infiltrating lymphocytes (TILs) OS lung metastatic accompanied by accumulation of exhausted T cells and regulatory T cells (Tregs). $CD3^+$ T cells from human OS lung metastatic exhibited lower proliferation than in primary tissue. Importantly, TAMs mainly comprise immunosuppressive M2 phenotype in OS metastasis. Mechanistically, we found that PD-1 of TAMs inhibits the phagocytic potency, further promoting the progression of OS metastasis. Therefore, the study provides a strong technical support for OS immunotherapy based on PD-1 inhibitors.

* Corresponding author. Bone and Soft Tissue Tumors Research Centre of Yunnan Province, Department of Orthopaedics, The Third Affiliated Hospital of Kunming Medical University (Yunnan Cancer Hospital), Kunming, Yunnan, 650118, China.

** Corresponding author.

*** Corresponding author.

E-mail addresses: wangxi1a2b@sina.com (X. Wang), xuyushan1019@126.com (Y. Xu), yaozhihong@kmmu.edu.cn (Z. Yao).

[1] These authors contributed equally to this work.

https://doi.org/10.1016/j.heliyon.2023.e23498
Received 5 July 2023; Received in revised form 16 October 2023; Accepted 5 December 2023
Available online 13 December 2023

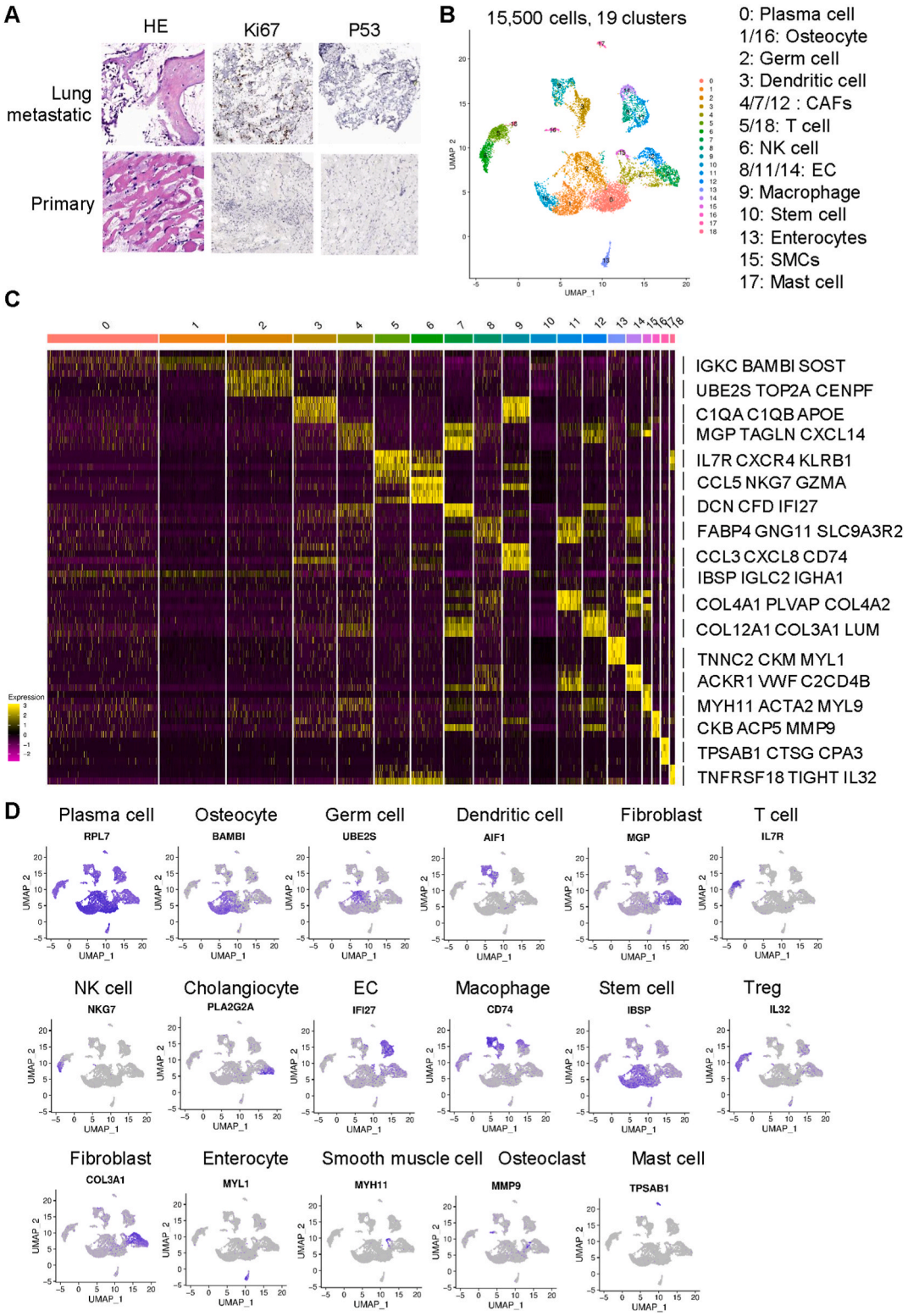

Fig. 1. Cellular constitution of human OS tumor lesions. (A) H&E and IHC analysis of infiltrated inflammation and Ki67, p53 in OS lung metastatic and primary tissue. **(B)** Uniform Manifold Approximation and Projection (UMAP) of scRNA-seq data from fresh OS lung metastatic patient. The color code for cell type assignment is indicated in the plot. **(C)** Heatmap analysis of gene expression in all cell clusters from B. **(D)** UMAP analysis of characterized genes in different clusters from B.

1. Introduction

Osteosarcoma (OS) is an uncommon bone malignancy, which is characterized by rapid growth, excessive metastasis. OS occurs mostly in children and adolescents under the age of 20, at approximately 8.7 per million people [1]. OS is most common in the distal femur, proximal tibia, the skull, mandible, pelvis, and vertebrae, and its incidence increases with age. The lung is the most common specific metastatic organ of osteosarcoma, and lung metastasis seriously affects the survival of patients with osteosarcoma [2]. The most effective treatment for OS is preoperative neoadjuvant chemotherapy combined with surgery and postoperative adjuvant chemotherapy [3]. Although the application of adjuvant chemotherapy has been paid more attention in clinical treatment, which has improved the survival rate to a certain extent, the 5-year overall survival rate is only 66.2 % [4], and with the higher recurrence or metastasis rate (higher than 30 %).

Recently, immunotherapy has shown excellent efficacy in a variety of malignant tumor [5,6]. For example, the antibody target PD-1 or programmed Cell Death-Ligand 1 (PD-L1) significantly improved the prognosis via reinvigorating the T cell activation or inducing the tumor cell death; However, the therapeutic effect of anti-PD-1/L1 on OS is limited [7,8]. Thus, it is urgent to clarify the molecular mechanism of the development and progress of OS and identify more effective therapeutic targets.

In recent years, single-cell sequencing technology has been an attractive strategy to map the role and function of different cells [9]. Compared with traditional sequencing methods, it is particularly important to solve the problems of low access and biological heterogeneity of biological materials. With this technology, researchers can study the development of OS with single-cell level, including tumor metastasis, tumor evolution and carcinogenesis, circulating tumor cells, etc. Single-cell RNA sequencing (scRNA-seq) has shown great application potential in illustrating intratumor heterogeneity in multiple cancers, even in the tumor microenvironment (TME) [10,11]. Factors such as cell type composition, developmental stage, and metabolic changes in the tumor immune microenvironment all affect the tumor progression [12].

In this study, we performed a comprehensive analysis of 15,500 qualified single-cell transcriptomes from 1 lung metastatic osteosarcoma lesion. Thirteen major cell clusters were identified, especially endothelial cells (ECs), cancer-associated fibroblasts (CAFs) and immune cells; transdifferentiation of malignant osteoblasts was further analyzed by trajectories. Furthermore, we found TILs in OS highly expressed exhaustion markers: including *TCF7*, *TOX* and *PDCD1*. Importantly, our study demonstrated that the PD-1 expression on TAMs inhibits the phagocytic potency, further promoting the progression of OS metastasis.

2. Results

2.1. Cellular constitution of human osteosarcoma tumor lesions

Apart from moderate survival rate of 66.2 % associated with the conventional chemotherapy for OS, it is also accompanying by high-rate recurrence/metastasis of less than 25 % of the 5-year overall survival rate. This could be attributed to the dynamic immunogenic characteristic of the tumor [13,14]. To explore the cellular constitution in osteosarcoma (OS), one lung metastatic OS sample was obtained, and rapidly digested to a single-cell suspension. After quality filtering, we clutered 15,500 cells from the tumor samples of OS patient (with lung metastasis). An increased lung metastasis was observed by H&E staining (Fig. 1A). Meanwhile, there are positive staining of Ki67 and p53 in the metastatic lung (Fig. 1A). One of the major mechanisms by which cancer weakens immune cells is via direct contact between PD-1 receptor on immune cells and PD-L1 expressed on tumor cell. Therefore, blocking either PD-1 or PD-L1 reinvigorate the effector cells and this has been identified as an emerging cancer immunotherapy approach. Macrophage is known to play important roles in the induction of antitumor immunity. However, it is controversial whether TAM in OS expresses PD-1 or not [15,16]. We analyzed the data by scRNA-seq analysis and identified 18 cell subgroups, mainly 13 cell types, according to the gene expression profiles, based on uniform manifold approximation and projection (UMAP) analyses and t-distributed stochastic neighbor embedding (t-SNE) (Fig. 1B). Furthermore, it has been established that the heterogeneity of TME is critical to treatment. Currently, clinical therapies in breast cancer are based on the molecular subtypes. Nonetheless, based on the available information, little is known about the heterogeneity of OS, and understanding it will improve our understanding of cancer immunotherapy. The

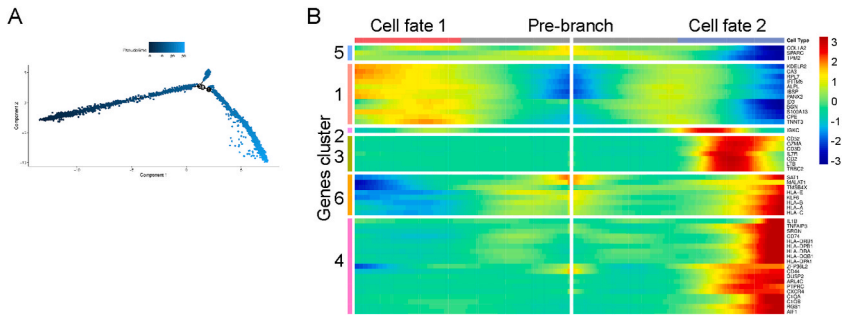

Fig. 2. Trajectory of OCs in human OS lesions. (A and **B)** Differentiation and developmental trajectories of OCs in OS, with different colors representing different cell types.

clusters were as follows: (1) T cells that are highly expressed with *CD3G, GZMA,* and *CD2*; (2) and (6), Plasma cells with high expressions of *IGHM, IGKC,* and *IGLC2*; (3) (5) and (8), Smooth muscle cells (SMCs) characterized with *TAC3, IGTA10,* and *ANO5* (4), Neutrophils that were highly expressed with *CTSG, CMA1,* and *MS4A2*; (7), Osteoblast with high expression of *IBSP, PTH1R,* and *GASS45G*, (9) Fibroblast characterized by *HP, MMP3,* and *SFRP1*; (10), Macrophages with specifically expressing of *IL1B, CXCL8,* and *C5AR1*; (11), Erythroid-like/precursor cells with *SELE, ACKR1,* and *EDN1* expressing; (12) (15) and (17), Endothelial Cells (ECs) were characterized by *ASPM, EBE2C,* and *CDC20*; (13), Dendritic cells (DCs) expressing *RBP7, FABP4,* and *SLC9A3R2* (Fig. 1C and D). These results revealed that heterogeneous cell subtypes that exhibited distinct molecular signatures.

2.2. Trajectory of osteoblastic cells maturation in human OS lesions

Osteoblastic cells (OCs) play a critical role in osteolysis in OS, which belongs to a multinucleated monocyte-macrophage lineage. We performed the trajectory analysis of the OCs by the Monocle 2 algorithm (Fig. 2A). The scRNA seq consists of series of steps from generation of single cell suspension, isolation of cells, cell barcoding and amplification, library preparation, sequencing and data analysis. Flow cytometry technique as well as immunohistochemistry were explained explicitly. Trajectory algorithms suggested that the signature patterns of the gene expression were in concordance with the six subclusters distribution. The transcription factors related to differentiation of chondroblastic cells, such as *COL2A1, SPARC,* and *TPM2*, were down regulated. In addition, the factors related to osteoblastic cells, such as *KDELR2, CA3,* and *RPL7*, also were down-regulated. Conversely, the genes related to immune cell response, which contains T cell activation (*CD52, GZMA, CD3D,* and *IL7R*), DC antigen processing (*SAT1, TMSB4X, KLF6,* and *IL7R*), macrophages (*IL1B, CD74, HLA-DRB1,* and *C1QA*), was upregulated in the process (Fig. 2B).

2.3. Diversity of ECs and CAFs in human OS lesions

ECs promote tumor angiogenesis and regulate immune response in TMEs. To explore the diversity of ECs in OS TME, we performed PCA analysis based on the gene expression profile, the data showed that there is three subclusters of ECs in the TMEs of OS lesions by t-SNE analysis, which were termed as the C0_*GNG11*$^{+}$ ECs, C1_*VMF*$^{+}$ ECs, C2_*COL4A2*$^{+}$ ECs, representing EC subcluster 8, 11, and 14. Next, we analyzed the expression characteristics for a set of featured genes in each EC subcluster (Fig. 3A and B) including: (1), C0_*GNG11*$^{+}$ ECs characterized with the expression of the proposed markers including *GNG11, FABP4,* and *SLC9A3R2* (Fig. 3B and C); (2) C1_*VMF*$^{+}$ ECs expressing with *NRAP, ANKRD1*, and *LMOD2* (Fig. 3B); (3) C2_*COL4A2*$^{+}$ ECs with highly expressing *PHOSPHO1, PANX3,* and *MT1G* (Fig. 3C). The distribution of the marker genes was showed by UMAP in Fig. 3D–F.

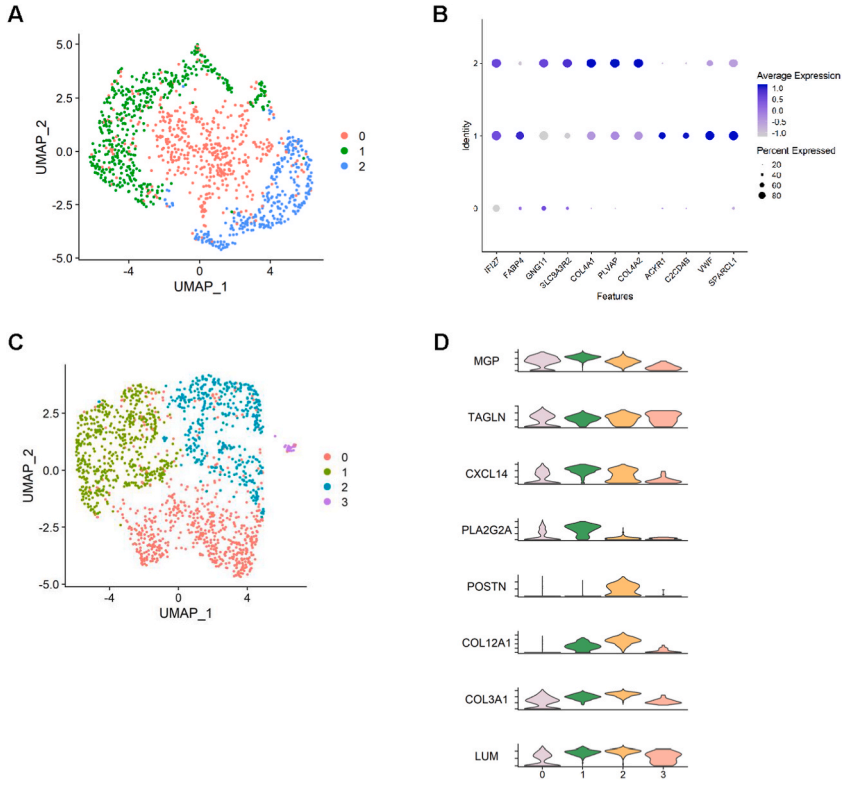

Fig. 3. Heterogeneity of ECs and CAFs populations in human OS lesions. (**A** and **B**) UMAP (**A**) and dot plot analysis (**B**) of characterized gene expression in ECs subsets from A. (**C** and **D**) UMAP (**C**) and violin plot analysis (**D**) of characterized gene expression in CAFs from C.

CAFs play the essential role in inducing tumor progression in several types of tumors. To understanding the role of CAFs in OS metastasis, we analyzed the heterogeneity of CAFs in OS patients. UMAP analysis showed that the CAFs can be divided into four subsets, which was characterized as C0_*MGP* + CAFs, C1_*CXCL14*$^{+}$ CAFs, C2_*POSTN*$^{+}$ CAFs, and C3_*LUM*$^{+}$ ECs, representing CAFs

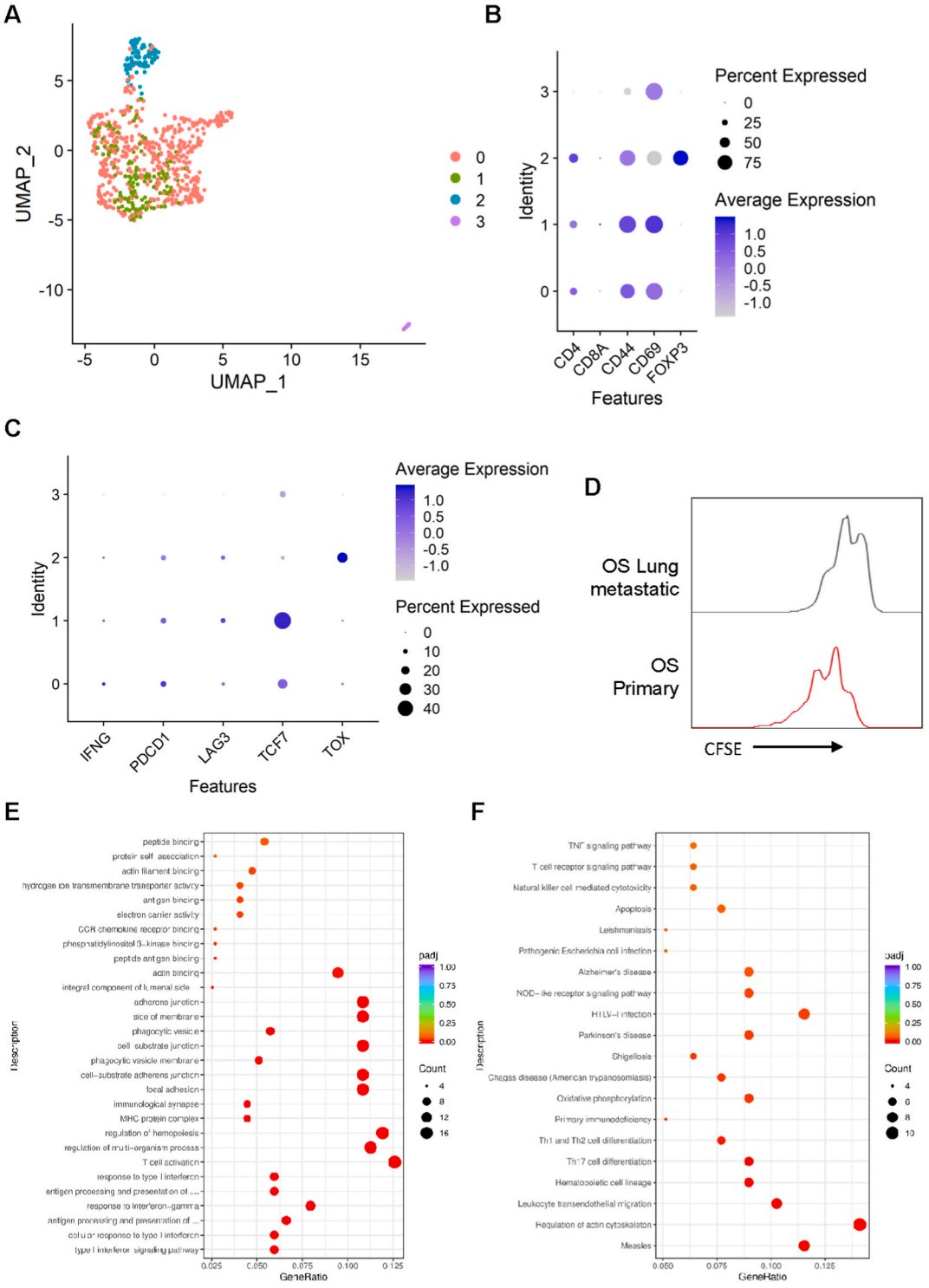

Fig. 4. Heterogeneity of TILs populations in human OS lesions. (**A**, **B** and **C**) UMAP (**A**) and dot plot analysis (**B** and **C**) of characterized gene expression in TILs subsets. (**D**) CFSE analysis of proliferation of CD3^{+} T cells from human OS lung metastatic and primary tissue. (**E** and **F**) Gene ontology (GO) (**E**) and KEGG enrichment analysis (**F**) in TILs subsets.

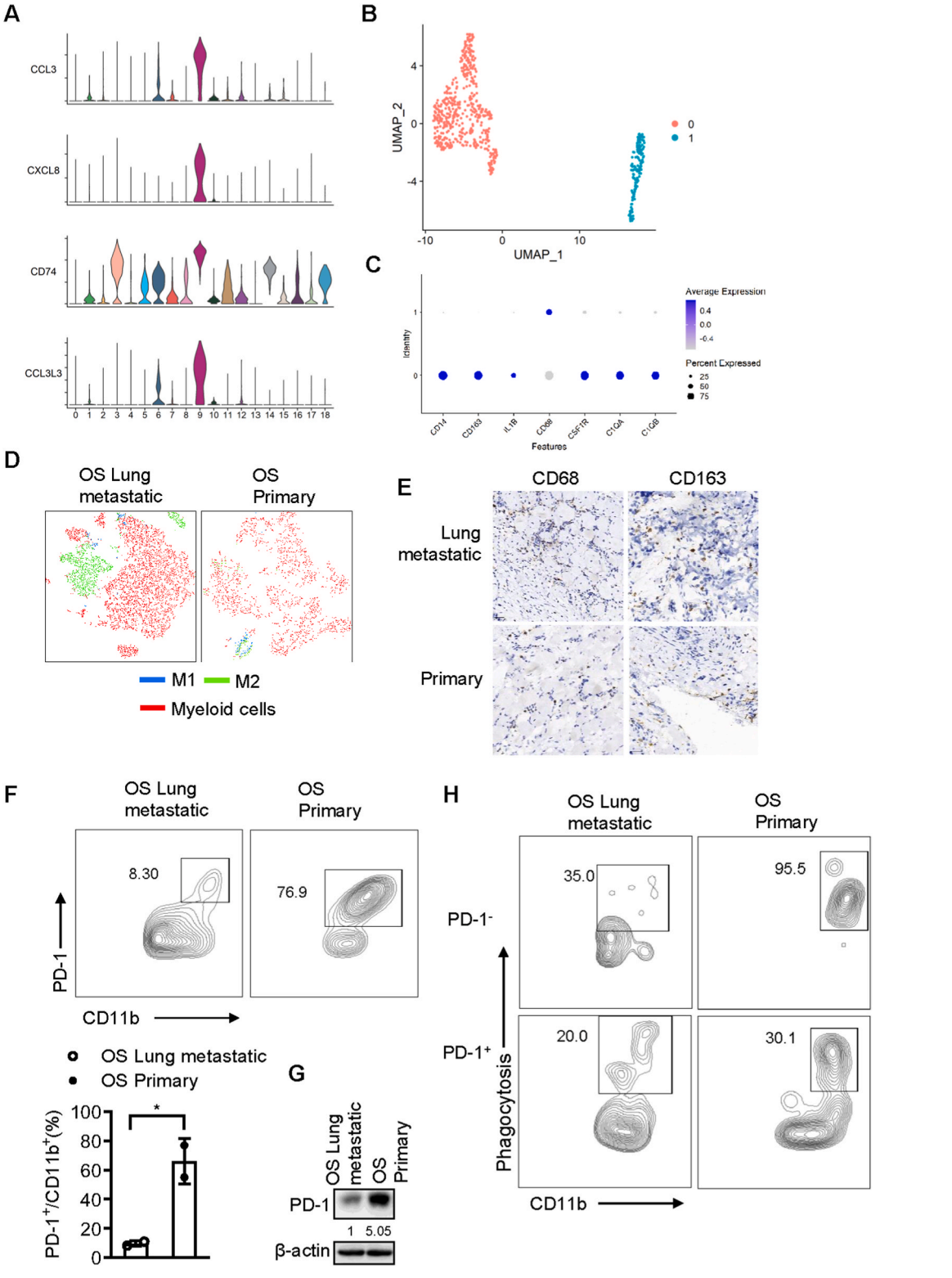

(caption on next page)

Fig. 5. The expression of PD-1 on TAMs inhibits the phagocytic activity in human OS lesisons. (**A**) Violin plot analysis of indicated gene expression in all cell cluster from human OS lesion. (**B** and **C**) UMAP (**B**) and dot plot analysis (**C**) of characterized gene expression in TAMs subsets from B. (**D**) Flow cytometry analysis of the TAMs subsets in human OS lung metastatic and primary tissue. (**E**) IHC analysis of CD68 and CD163 in tissues as mentioned in D. (**F** and **G**) Flow cytometry analysis (F) and Western blot analysis (G) of PD-1 expression on TAMs from the indicated groups. The immunoblot shows a normalized expression of PD-1 to β-actin. The protein expression of PD-1 was calculated by Image J. (**H**) Flow cytometry analysis of phagocytic potency from PD-1$^-$ and PD-1$^+$ TAMs in tissues as mentioned in D.

subcluster 4, 7, and 12 (Fig. 3C). In addition, the expression characteristics for CAFs subcluster including: (1), C0_*MGP*$^+$ CAFs characterized with the expression of the proposed markers including *MGP* and *TAGLN* (Fig. 3B and C); (2) C1_*CXCL14*$^+$ CAFs expressing with *CXCL14* and *PLA2G2A,* which are associated with regulation of immune cell migration; (3) C2_ *POSTN*$^+$ CAFs with highly expressing *POSTN* and *COL12A1;* (4) C3_ *LUM*$^+$ CAFs with highly expressing *COL3A1* and *LUM* (Fig. 3D). These results revealed that the presence C1_ *CXCL14*$^+$ CAFs have the ability to regulate the anti-tumor ability.

2.4. Heterogeneity of tumor-infiltrating lymphocytes (TILs) in human OS lesions

Given that T cells are the major type of lymphocytes in the TME, which are essential in cancer immunotherapy. We identified that there are four subcluster TILs in the TME, including: (1) C0_*CD44*$^+$ T cells characterized with the expression of the T cell activation markers: *CD44* and *CD69,* which maintained T cell proliferation and activation; (2) C1_*TCF7*$^+$ T cells characterized with the expression of *TCF7* and *PDCD1,* which are associated with T cell exhaustion; (3) C2_*Foxp3*$^+$ T cells with highly expressing *CD4* and Foxp3, which is the transcription factor of Tregs*;* (4) C3_*CD69*$^+$ T cells with highly expressing *CD69* and *TCF7* (Fig. 4A–C). Importantly, we also noticed that TILs expressed high levels of the T cell exhaustion-related genes, *TCF1, TOX* and *PDCD1* (Fig. 4C).

Furthermore, to confirm the TILs proliferation in OS patients, we isolated TILs from OS lung metastatic and primary tissue, CFSE data showed that the proliferation of TILs was much lower in lung metastatic than in primary tissue (Fig. 4D). KEGG pathway analysis showed that TILs in the OS lesions related to antigen processing and presentation of T cells, MHC protein complex (Fig. 4E). Consistent with the data, GO analysis showed the expression of genes that related to T cell activation, regulation of hemopoiesis, regulation of multi-organism process, were enriched in the TILs (Fig. 4F), the pathway which participates the regulation of actin cytoskeleton was predominantly enriched in T cells, and most of the pathways were correlated with T cell fate and anti-infection immunity (Fig. 4F).

2.5. Heterogeneity of tumor-associated macrophages (TAMs) in human OS lesions

Tumor-infiltrating myeloid cells were characterized with tumor promoting and suppressing function, which plays critical roles in TME. Analysis of the macrophages showed that TAMs specifically highly expressing *CCL3, CXCL8, CD74,* and *CCL3L3* (Fig. 5A). We identified two subsets of TAMs including: (1) C0_*CD163*$^+$ TAMs characterized with M2 markers including *CD163* and *IL1B,* which are associated with anti-tumor immunity; (2) C1_*CD68*$^+$ TAMs characterized with the expression of *CD68* and *CSF1R,* which mediate M1 pro-inflammatory response (Fig. 5B and C). Consistently, we detected the percentage of M1 and M2 in OS patients, flow cytometry (FCM) analysis revealed the percentage of M2 were much higher in OS lung metastatic than in primary tissue (Fig. 5D). Immunohistochemistry (IHC) data confirmed that CD163 expression was higher in OS lung metastatic than in primary tissue (Fig. 5E). These data revealed that TAMs in the OS metastatic highly expressing CD163, which is the marker of M2 macrophages.

2.6. Expression of PD-1 mitigates phagocytic activities TAM in osteosarcoma

Amounting evidence have demonstrated that TAMs correlate with poor prognosis in cancer patients. However, is remains unclear

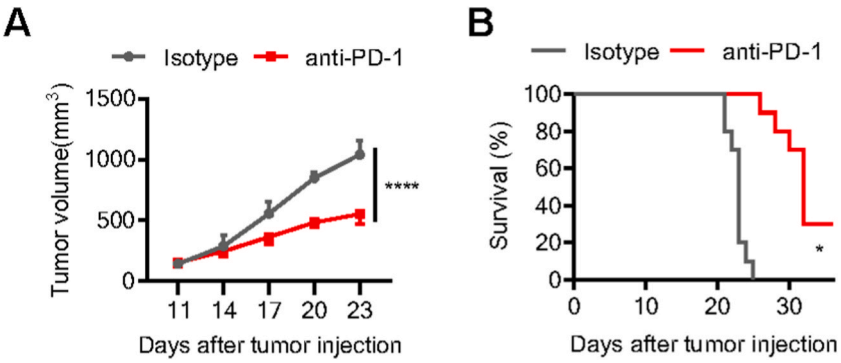

Fig. 6. PD-1 inhibitor suppresses the tumor growth in OS mouse model. (**A** and **B**) The tumor growth (**A**) and survival analysis (**B**) in nude mouse injected s.c. with 431B OS cells followed by intraperitoneal (i.p.) injection with PD-1 (RMP1-14) antibody on days 0, 4, 7 and then every third day. In (A), data are representative of 3 independent experiments, mean ± SD. *$P < 0.05$; ****$P < 0.0001$. Two-way ANOVA in (**A**, n = 10), log-rank (Mantel-Cox) test in (**B**, n = 10)].

that the percentage of M1 or M2 in OS could correlate with OS metastatic? Given that PD-1 expression on TAMs correlates negatively with phagocytic activity against colon cancer cells, we wondered whether the TAMs in OS patients could express PD-1, if so, what consequences of PD-1 expression could have on the OS metastatic. Firstly, we isolated immune cells from OS patients' tissue to examine the PD-1 expression on TAMs. FCM and Western blot analysis showed the expression of PD-1 on TAMs was much lower in OS lung metastatic tissue than in primary tissue, indicating that PD-1 expression on TAMs may positively correlate with OS metastatic (Fig. 5F and G). Beyond the function of PD-1 in inhibiting the effectorT cells, we hypothesized that the expression of PD-1 may influence TAM phagocytic activity by suppresing the effector functions of activated TAMs. To compare the phagocytotic activity of PD-1^+ versus PD-1^- TAMs by FCM analysis, data showed that PD-1^- TAMs phagocytosed more BioParticles *in vitro* than PD-1^+ TAMs in OS lung metastatic and primary tissue (Fig. 5H). In addition, compared to OS primary tissue, PD-1^- TAMs or PD-1^+ TAMs in OS lung metastatic tissue phagocytosed less BioParticles *in vitro* (Fig. 5H). These results demonstrated that PD-1 expression on TAMs negatively correlates with the phagocytic activity, further promoting the progression of OS metastasis.

Furthermore, to confirm the role of PD-1 on the effect of OS, we conducted OS mouse model, and the tumor-bearing mice was administrated with anti-PD-1. The data showed that anti-PD-1 inhibited the tumor growth, and increased the survival (Fig. 6A and B). Altogether, our study showed a potential role of PD-1 inhibitor in OS.

3. Discussion

Our finding provides a comprehensive understanding the expression of PD-1 on TAMs phagocytosis activity in OS metastasis. The data showed that PD-1 may inhibit the phagocytosis potency of TAMs in OS. Consistent with the function of PD-1 on T cells. Furthermore, the data showed that the phagocytosis potency of PD-1^- TAMs is much weaker in OS lung metastasis tissue than in primary tissue, indicating that the expression of PD-1 on TAMs may participate the metastasis progression.

We showed the phenotype of ECs and immune cell clusters in the TMEs in OS. We found that there are three subclusters, identified as *CDC20*$^+$ ECs, *ANKRD1*$^+$ ECs, *PANX3*$^+$ ECs, promoting the tumor metastasis in OS patients. ECs promote tumor proliferation and growth by inducing the recruitment of blood vessels. Targeting ECs metabolism can be an alternative to overcome the failure of anti-antigenic therapies. Previous study has not only showed that TME expressed NK7, but also express TIGHT, which is a promising target in cancer immunotherapy [17]. Our study revealed that the ECs in the TME may promote the angiogenesis in OS patients. Our data supported that targeting *CDC20* may be a potential novel target in OS [18]. Furthermore, we identified two novel tumor ECs in OS: *ANKRD1*$^+$ ECs, *PANX3*$^+$ ECs.

We showed that T cell clusters in the OS patients could express the NK cell markers *NKG7,* which is a characteristic of cytotoxic CD8$^+$ T cells, could mediate complete response to anti-PD-1 therapy. Previous study also showed that T cell in TME express *NKG7,* but also express *TIGHT*, which is a promising target in cancer immunotherapy [19]. As we know, anti-PD-1 could overcome the T cell inhibitory response, got great clinical outcome, however, previous studies showed that OS patients cannot response to anti-PD-1 therapy. Our study proposed a novel combination in the OS patients that anti-NKG7 may be a potential combination for anti-PD-1.

Our data showed that two subsets of TAMs including: (1) C0_*CD163*$^+$ TAMs characterized with M2 markers including *CD163* and *IL1B,* which are associated with anti-tumor immunity; (2) C1 *CD68*$^+$ TAMs characterized with the expression of *CD68* and *CSF1R,* which mediate M1 pro-inflammatory response. One major limitation of scRNA-seq is high dropout rate which is usually very difficult to solve. In this study, we demonstrate the phenotypes of ECs, CAFs and immune cells in OS patient by binarizing scRNA seq count data. We demonstrated that the scRNA seq technology is a powerful strategy to illustrate the TME phenotypes.

TAMs in the OS patients got be conversed in past decades, which is M1 or M2 macrophages in the TME [20,21]. *In vivo* experiments showed that the culture supernatants derived from OS-stimulated M1 macrophages significantly inhibited the growth of OS [22]. Meanwhile, M2 macrophages may promote extracellular matrix remodeling and angiogenesis. In tumors, TAMs are usually differentiated into M2 state by environmental factors [23]. Consistently, our data showed that M2 macrophages is the major TAMs in OS patients. Together, our data depicts the comprehensive ECs and TAMs in the OS TME. And also proposed potential target to the immunotherapy for OS.

4. Methods

4.1. Approval of studies and patient informed consent

Six patients admitted to Yunnan Cancer Hospital during December 2021 to December 2022 were enrolled in this study. There are 6 OS patients, five patients were female, one patient was male, was aged from 9 to 43 years, with the average of (17.83 ± 12.54) years.

4.2. Declarations

The study were reviewed and approved by the Ethics Committee of The Third Affiliated Hospital of Kunming Medical University (Yunnan Cancer Hospital) (No. KYLX2022133). All methods in this study were carried out in accordance with relevant guidelines and regulations. Written informed consent was obtained from all participants.

5. Sample preparation and cell isolation for RNA-Seq

Fresh tumor tissue was soaked in a 10 cm dish containing tissue preservation solution and placed on ice for processing. Samples

were washed 3 times with Hanks' Balanced Salt Solution (HBSS), then cut into 1–2 mm tissue fragments, and surgical forceps were used to remove connective tissue and obvious necrotic tissue. Digest tissue fragments with GEXSCOPETM tissue dissociation solution (Singleron) for 15 min at 37 °C with agitation. The processed samples were filtered through a 40 μm sterile filter and centrifuged at 800×*g* for 5 min. The supernatant was discarded, and then the cell pellet was resuspended with phosphate-buffered saline (PBS; Gibco, USA), and erythrocytes were immediately removed by the addition of 2 mL of GEXSCOPETM erythrocyte lysis buffer (Singleron). The cell suspension was incubated at 25 °C for 10 min, then centrifuged at 500×*g* for 5 min and resuspended in PBS. Samples were stained with trypan blue (Gibco, USA) and was assessed under phase contrast light microscopy (Olympus, Japan).

5.1. Library preparation and scRNA-Seq

Single-cell-containing master mixes were prepared with a Chromium Controller (10 × Genomics), and scRNA-seq libraries were constructed using the Chromium Single Cell 3′ Library, Gel Bead & Multiplex Kit (10 × Genomics, V2, and V3) according to the manufacturer's instructions. Depending on sample volume requirements, cells were examined with a light microscope, and then counted with a hemocytometer. Next, cells were added to each channel, and the number of channel cells was approximately 5000 cells. Cell lysis and barcoded reverse transcription of RNA followed by cDNA amplification were performed in single-cell gel bead emulsions. Illumina HiSeq X Ten instrument (Illumina, Inc) were used to sequence the single-cell libraries.

5.2. Pre-processing of scRNA-Seq data

Log in to the server and install the CellRanger 4.0 tool (https://www.10xgenomics.com/) under the CentOS 8 operating system, modify the sequencing file name to the standard format and download the human reference transcriptome package pre constructed by 10x genomics。These include human reference genome FASTA file (grch38 release 98) and human reference genome annotation GTF file (gencode version 32). Run the cell Ranger count tool to compare the data, remove empty droplets, and generate a single cell count matrix.

Download and install the R program (version 3.6.3) and the Seurat package (version 3.1.5) and process the raw output data for each sample [24]. Perform quality control on the single-cell count matrix, and include cells with gene types >500, library size >1000, and mitochondrial proportion <20 % as cells with qualified data quality and included in downstream analysis, and exclude cells expressing <10 cells in each sample. Gene. Totally, we perform further bioinformatics analysis using 15,500 filtered cells.

5.3. Data integration and the dimensionality reduction

Normalization was performed using the Seurat package SCTransform to minimize the impact of library size and gene expression abundance on the analysis. SCTransform uses residuals after model fitting for subsequent identification of highly variable genes, data scaling, principal component analysis, unsupervised clustering and visual dimensionality reduction. Then logarithmically normalized using the Seurat package NormalizeData. The top 3000 genes with the largest residual variance after SCTransform normalization were further selected as highly variable genes. Scale the residuals of the above hypervariable genes to data with a mean of 0 and a standard deviation of 1, ensuring that each gene has the same weight in the analysis. The scaled highly variable gene matrix can be further reduced by principal component analysis, which extracts the variation in the data by means of orthogonal transformation. Principal component analysis was done using the Seurat package RunPCA, and the top 50 principal components were selected for subsequent graph-based unsupervised clustering and nonlinear dimensionality reduction data visualization.

6. Cell clustering and annotation

To perform cluster analysis on the normalized data by the Louvain algorithm, and the tSNE(t-distributed stochastic neighbor embedding) [25] function in the Seurat package was used for nonlinear dimensionality reduction. Then, apply the tSNEPlot function to plot the tSNE cell clusters. The DEGs of all clusters were analyzed using the Wilcoxon algorithm, and the DEGs were scored in a group one vs rest method. Genes that were specifically highly expressed, logFC >0.25, and expressed in at least 20 % of cells per cluster were selected as significant DEGs for the cluster. Cell types were annotated using the single-cell sequencing cell type annotation software Single R combined with DEGs.

6.1. DEGs identification and GO enrichment analysis

The Wilcoxon rank sum test with the FindMarkers function in Seurat (adjusted P-value <0.05, logfc.threshold = 0, 1 and only.pos = T) were used to identifing differentially overexpressed in a particular cluster compared to the rest of the remaining clusters Gene and cluster-specific overrepresentation of biological processes for GO were calculated using the CompareCluster function in the ClusterProfiler package (version 3.14.3) for R cell clusters. Download the human GO and KEGG datasets as the target gene set from the official website, and then prepare the files to be imported by the GSEA software. To identify pathways that are induced or repressed across cell clusters by GSEA with curated gene sets (https://www.gsea-msigdb.org/gsea/msigdb). Average gene expression levels were calculated and log 2-fold change (FC) between cell clusters. To assess relative pathway activity in T, macrophages, and DC cells, we also applied Gene Set Variation Analysis (GSVA) The list of signature genes for T cells (naive, costimulatory, cytotoxic, exhausted) and TAMs (M1, M2) was taken from Chung et al. [26]. A genomic list of IFN-γ pathway activity and DC activity in T cells was obtained from the

MSigDB collection.

6.2. Sing-cell copy-number variation and clonality analysis

The inferCNV algorithm was used to detect large copy number gains or deletions covering multiple genes at the single-cell genome level. It is hypothesized that the relative differences in transcript expression between tumor and normal cells are regulated by transcriptional machinery or caused by genomic copy number alterations. By using immune cells as a reference, the CNVs of osteoblast and chondrocyte tumor cells were calculated. Prepare single-cell raw count matrix, annotation information for reference cell type and cell type to be tested, gene coordinates and chromosomal location files. Genes with mean expression values less than 0.1 were then filtered, and gene expression levels were normalized and log-transformed based on the median library size across all cells. A standard Bayesian latent mixture model was used to reduce false-positive CNV calls(default value of 0.5 as the threshold). To infer changes in cloned single-cell CNVs, subcluster cells were inferred from HMM-generated CNV values using the "subcluster" method. Given the genomic information of the cellular bands, any changes in the p or q arm levels can simply be translated into equivalent CNVs depending on their location. After that, subclones containing the same arm-level CNVs were folded and the tree reorganized to represent the subclone CNV architecture. The data visualization adopts the UPhyloplot2 algorithm [27] (https://github.com/harbourlab/UPhyloplot2), which is used to automatically generate the intratumoral evolutionary tree. Arm-level CNV calls were used as input.

6.3. Trajectory analysis of single cells

Single-cell pseudo-time trajectories were generated in R using the Monocle3 package. Use the raw UMI count ratio gene-cell matrix from Seurat processed data as input. The new Cell Data Set function is used to create an object of the parameter expression Family = negbinomial size. Only genes (mean expression $\geq$0.1) were used in trajectory analysis and dimensionality reduction was performed on DEGs between cell groups. Use the plot cell trajectory function to classify and visualize cells. Use plot pseudotime heatmap to calculate and visualize genes at pseudotime (q-val <10-10) and group genes into subgroups based on gene expression patterns. Genes with q-values <10-10 resulting from the Branch Expression Analysis Modeling (BEAM) analysis were grouped and plotted using the visualized plot genes branched heatmap function. The enriched GO terms were calculated using the Cluster Profilter package (version 3.14.1). Retrieve differentially expressed transcription factors from a list of DEGs. The SCORPIUS algorithmwas used to deduce the linear transformation of Monocle 3-derived OCs from OC precursors and immature OC cells to mature OCs in OS tissues.

6.4. Flow cytometry analysis of PD-1 expression on TAMs

Tumor-infiltrated immune cells were isolated using Percoll from OS patients, washed cells 2 times with pre-warmed PBS, then the cells were stained with Live/Dead (APC-Cy7), and anti-CD11b (Percp-cy5.5), anti-PD-1 (BV421) for 15 min at 4 °C, washed with pre-warmed PBS for 1 time. BD LSRFortessa was used to acquire data, TreeStar was used for the FCM data analysis.

6.5. CellTrace CFSE analysis of TILs proliferation

Tumor-infiltrating lymphocytes were isolated using Percoll from OS patients, washed with pre-warmed PBS for 2 times, followed by re-suspended with CFSE working solution (5 μM, Thermo Fisher, C34554), stained 20 min at 37 °C water bath, added 6–8 ml pre-warmed PBS and incubated for 5 min, 300 g centrifuge 5 min and washed with pre-warmed PBS for two times. 72 h later, cells were washed and stained with Live/Dead (APC-Cy7) and anti-CD3 (FITC). BD LSRFortessa was used to acquire data, TreeStar was used for the FCM data analysis.

7. Immunohistochemistry (IHC) analysis with TAMs

Tissues were fixed with 8 ml 4 % paraformaldehyde. To obtain OCT frozen sample or paraffin-embedded sample, tissue sections were cut into 6 μm or 5 μm slices. The primary antibodies were used: CD68 (Abcam, ab125047) diluted 1:400, CD163 (Abcam, ab87099) diluted 1:200, Ki67 (Abcam, ab15580) diluted 1:500, p53 (Abcam, ab131442) diluted 1:400. Sections were then cultured with the corresponding secondary antibodies (goat anti-rabbit IgG antibody (H + L), biotinylated (Vector Laboratories, number BA-5000; diluted 1:200). The signal was acquired with Aperio Digital Pathology according to the manufacturer's instructions.

7.1. Western blot analysis of PD-1 expression

Tumor-infiltrating lymphocytes were isolated using Percoll from OS patients, washed with PBS for 2 times, TAMs were sorted by MACS with CD11b magnetic beads. Then the cells were lysed with RIPA, collected the supernatant after centrifuge, the supernatant protein concentration was calculated by Pierce Rapid Gold BCA kit (Thermo Fisher Scientific, A53225). Totol 25 μg protein was loaded to 10 % SDS PAGE, and transferred to 0.45 μM (Thermo Fisher Scientific, 88518). The protein was imaged by ECL. And the data was analyzed by Image J.

7.2. OS bearing tumor mouse model and anti-PD-1 administration

Nude mouse was injected s.c. with 431B OS cells, 7 days later, mouse was randomized divided into two group, then injection with PD-1 (RMP1-14) antibody by intraperitoneal (i.p.) on days 0, 4, 7 and then every third day. Tumor volume was measured every 3 days from day 7, and the animal survival rates were recorded. Tumor volume was calculated as follows: length × width × width × 0.5. The tumor-bearing mice with tumor sizes larger than 20 mm were euthanized for ethical considerations.

Data availability statement

The data that support the findings of this study are available from the corresponding author upon reasonable request. The scRNA sequencing data have been deposited in NCBI's Gene Expression Omnibus (GEO) and are accessible through accession number GSE234187 (https://www.ncbi.nlm.nih.gov/geo/query/acc.cgi?&acc=GSE234187).

CRediT authorship contribution statement

Chenhong Zheng: Investigation, Data curation and Methodology. **Heng Li:** Data curation. **Xiaohui Zhao:** Investigation. **Siyu Yang:** Investigation. **Jinqin Zhan:** Visualization. **Huaie Liu:** Formal analysis. **Yan Jiang:** Software. **Li shi:** Investigation. **Yaxian Song:** Investigation. **Yujie Lei:** Methodology. **Tingdong Yu:** Formal analysis. **Xiaoxiong Wang:** Visualization. **Hongsheng Li:** Investigation. **Xi Wang:** Resources. **Yushan Xu:** Resources. **Zhihong Yao:** Validation and Resources.

Declaration of competing interest

Authors declare that they have no competing interests.

Acknowledgements

This study is supported by the National Natural Science Foundation of China (Nos. 82160125 to ZCH, 81960488 to YZH); the Joint Special Funds for the Department of Science and Technology of Yunnan Province Kunming Medical University (No. 202001AY070001-195, 149,150; 202201AY070001-168,170,136,041,160); the Science and Technology Innovation Team of Diagnosis and Treatment for Glucolipid Metabolic Diseases in Kunming Medical University (No. CXTD202106); the Yunnan Provincial Department of Education Science Research Fund Project (Nos. 2020J0197, 2022J0235, 2021J0263, 2023Y0654 and 2019EF001 [−236]); Start Up Fund for Doctoral Research of Hohhot First Hospital [No. 2023SYY(BS)019]; and Yunnan Fundamental Research Projects (No. 202101AY070001-[171]). The National Cancer Center Climbing Fund of China [NCC201925B02]. 535 Talent Project of First Affiliated Hospital of Kunming Medical University (2023535D14). The Medical Reserve Talents of Yunnan Province (No. H-2019072).

References

[1] A. Misaghi, et al., Osteosarcoma: a comprehensive review, SICOT J 4 (2018) 12.
[2] A.J. Saraf, J.M. Fenger, R.D. Roberts, Osteosarcoma: accelerating progress makes for a hopeful future, Front. Oncol. 8 (2018) 4.
[3] H. Koksal, et al., Treating osteosarcoma with CAR T cells, Scand. J. Immunol. 89 (3) (2019), e12741.
[4] M.A. Duggan, et al., The surveillance, epidemiology, and end results (SEER) program and Pathology: toward strengthening the critical relationship, Am. J. Surg. Pathol. 40 (12) (2016) e94–e102.
[5] Y. Suehara, et al., Clinical genomic sequencing of pediatric and adult osteosarcoma reveals distinct molecular subsets with potentially targetable alterations, Clin. Cancer Res. 25 (21) (2019) 6346–6356.
[6] D. Wang, et al., Multiregion sequencing reveals the genetic heterogeneity and evolutionary history of osteosarcoma and matched pulmonary metastases, Cancer Res. 79 (1) (2019) 7–20.
[7] A. Le Cesne, et al., Programmed cell death 1 (PD-1) targeting in patients with advanced osteosarcomas: results from the PEMBROSARC study, Eur. J. Cancer 119 (2019) 151–157.
[8] P. Thanindratarn, et al., Advances in immune checkpoint inhibitors for bone sarcoma therapy, J Bone Oncol 15 (2019), 100221.
[9] K. Mulder, et al., Cross-tissue single-cell landscape of human monocytes and macrophages in health and disease, Immunity 54 (8) (2021) 1883–1900 e5.
[10] I. Tirosh, et al., Dissecting the multicellular ecosystem of metastatic melanoma by single-cell RNA-seq, Science 352 (6282) (2016) 189–196.
[11] H.W. Lee, et al., Single-cell RNA sequencing reveals the tumor microenvironment and facilitates strategic choices to circumvent treatment failure in a chemorefractory bladder cancer patient, Genome Med. 12 (1) (2020) 47.
[12] M.Z. Noman, et al., Improving cancer immunotherapy by targeting the hypoxic tumor microenvironment: new opportunities and challenges, Cells 8 (9) (2019).
[13] L. Hu, W. Wu, J. Zou, Circular RNAs: typical biomarkers for bone-related diseases, J. Zhejiang Univ. - Sci. B 23 (12) (2022) 975–988.
[14] Q. Liu, et al., miR-29 promotes osteosarcoma cell proliferation and migration by targeting PTEN, Oncol. Lett. 17 (1) (2019) 883–890.
[15] A.L. Cesne, et al., Safety and efficacy of Pazopanib in advanced soft tissue sarcoma: PALETTE (EORTC 62072) subgroup analyses, BMC Cancer 19 (1) (2019) 794.
[16] P. Thanindratarn, et al., Establishment and characterization of a recurrent osteosarcoma cell line: OSA 1777, J. Orthop. Res. 38 (4) (2020) 902–910.
[17] L. Nagl, et al., Tumor endothelial cells (TECs) as potential immune directors of the tumor microenvironment - new findings and future perspectives, Front. Cell Dev. Biol. 8 (2020) 766.
[18] Z. Wang, et al., Cdc20: a potential novel therapeutic target for cancer treatment, Curr. Pharmaceut. Des. 19 (18) (2013) 3210–3214.
[19] Y. Zhou, et al., Single-cell RNA landscape of intratumoral heterogeneity and immunosuppressive microenvironment in advanced osteosarcoma, Nat. Commun. 11 (1) (2020) 6322.
[20] G. Germano, et al., Role of macrophage targeting in the antitumor activity of trabectedin, Cancer Cell 23 (2) (2013) 249–262.
[21] A. Lopez-Janeiro, et al., Prognostic value of macrophage polarization markers in epithelial neoplasms and melanoma. A systematic review and meta-analysis, Mod. Pathol. 33 (8) (2020) 1458–1465.
[22] A. Maccio, et al., Role of M1-polarized tumor-associated macrophages in the prognosis of advanced ovarian cancer patients, Sci. Rep. 10 (1) (2020) 6096.

[23] P. Dhupkar, et al., Anti-PD-1 therapy redirects macrophages from an M2 to an M1 phenotype inducing regression of OS lung metastases, Cancer Med. 7 (6) (2018) 2654–2664.
[24] A. Butler, et al., Integrating single-cell transcriptomic data across different conditions, technologies, and species, Nat. Biotechnol. 36 (5) (2018) 411–420.
[25] T. Stuart, R. Satija, Integrative single-cell analysis, Nat. Rev. Genet. 20 (5) (2019) 257–272.
[26] W. Chung, et al., Single-cell RNA-seq enables comprehensive tumour and immune cell profiling in primary breast cancer, Nat. Commun. 8 (2017), 15081.
[27] M.A. Durante, et al., Single-cell analysis reveals new evolutionary complexity in uveal melanoma, Nat. Commun. 11 (1) (2020) 496.